Fullerenes, Nanotubes, and Carbon Nanostructures, 20: 1–16, 2012

ISSN: 1536-383X print / 1536-4046 online
DOI: 10.1080/1536383X.2011.586618

Taylor & Francis
Taylor & Francis Group

One-Dimensional Uneven Peanut-Shaped C_{60} Polymer: A Quantum Electronic System in Riemannian Space

JUN ONOE[1], TAKAHIRO ITO[2], SHIN-ICHI KIMURA[2], HIROYUKI SHIMA[3], YASUHIRO TODA[3] AND HIDEO YOSHIOKA[4]

[1]Research Laboratory for Nuclear Reactors, Tokyo Institute of Technology, Tokyo, Japan
[2]UVSOR Facility, Institute for Molecular Science and School of Physical Science, The Graduate University of Advanced Studies (SOKENDAI), Okazaki, Japan
[3]Division of Applied Physics, Faculty of Engineering, Hokkaido University, Sapporo, Japan
[4]Department of Physics, Nara Women's University, Nara, Japan

When a C_{60} film is irradiated with a 3 kV electron-beam in an ultrahigh vacuum (base pressure: 10^{-7} Pa), C_{60} molecules are coalesced to form a one-dimensional (1D) uneven peanut-shaped C_{60} polymer. From a topological viewpoint, since the polymer has both positive and negative Gaussian curvatures, it can be regarded as a new allotrope of nanocarbons different from graphene, fullerenes, and nanotubes. We will present our recent results of the electronic, optical, and electron-transport properties of the 1D uneven peanut-shaped C_{60} polymer and discuss its novel electronic properties on the basis of quantum mechanics in Riemannian space.

Keywords One-dimensional uneven peanut-shaped C_{60} polymer, gaussian curvature, electronic properties, optical properties, electron-transport properties

Introduction

Since the first report on C_{60} photo-polymerization (1), there have been many reports on C_{60} polymers obtained using various kinds of methods, as shown in Table 1 (2). We have produced C_{60} polymers from photo and electron-beam (EB) irradiation of pristine C_{60} films and investigated their structural and electric properties. As shown in Figure 1, photo-polymerization provides two-dimensional (2D) semiconducting dumbbell-shaped C_{60} polymers (left) with a resistivity of 10^3 Ωcm (3–9), whereas EB-polymerization does metallic peanut-shaped C_{60} polymers with that of 1–10 Ωcm (10–18). These resistivity

This article was part of the Proceedings of the 9th Biennial International Workshop "Fullerenes and Atomic Clusters" held in 2009 in St. Petersburg, Russia. Other articles in the proceedings were previously published in *Fullerenes, Nanotubes, and Carbon Nanostructures* 18(4–6) and 19(1–2).

Address correspondence to Jun Onoe, Research Laboratory for Nuclear Reactors, Tokyo Institute of Technology, O-okayama, Meguro, Tokyo 152-8550, Japan. E-mail: jonoe@nr.titech.ac.jp

Table 1
Summary of fullerene polymers obtained using various methods

Method	Reactant	Cross-linkage	Structure
Photo-irradiation	C_{60} film	dumbbell	1D
		single-bond	2D hexagonal
			1D
High-Temperature and high- pressure	Solid C_{60}	dumbbell	1D orthorhombic
			2D tetragonal
			2D hexagonal
			3D tetragonal/ hexagonal
Charge transfer	AC_{60}*	dumbbell	1D orthorhombic
	Na_2RbC_{60}	single-bond	1D orthorhombic
	Na_4C_{60}	single-bond	2D tetragonal
Solid catalysis	C_{60} powder KCN	dumbbell	dimer/trimer
Electron-beam	Solid C_{60}	dumbbell	dimer
	C_{60} film	peanut-shaped	1D
		dissociation	3D amorphous

*A denotes alkali metals.

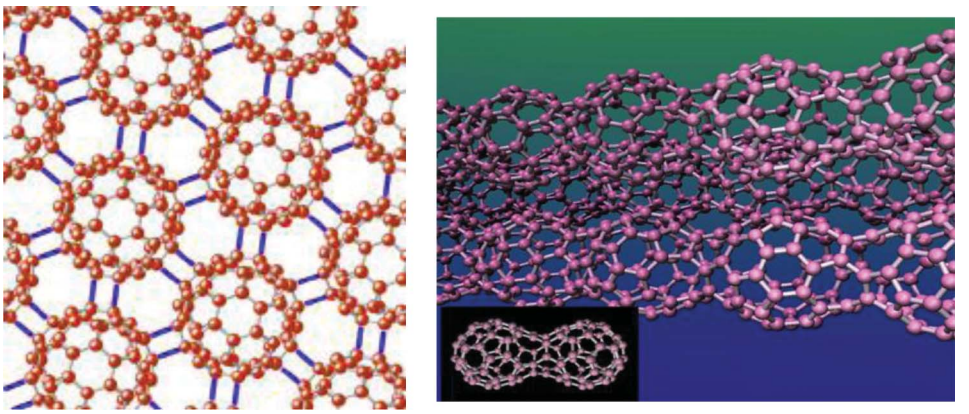

Figure 1. Schematic illustration of 2D hexagonal dumbbell-shaped C_{60} polymers (left) and 1D uneven peanut-shaped C_{60} polymer (right) (taken from Refs. 11 and 14) (color figure available online).

values were obtained using four-probe measurements at room temperature under atmospheric conditions, which are much smaller than that of 10^8–10^{14} Ωcm of solid C_{60} (19,20).

As shown in Figure 1 (left), the 2D C_{60} polymer has a [2 + 2] four-membered cross-linkage between adjacent C_{60} molecules by dissociation of C = C double bonds of each C_{60}. In this case, the whole system is not regarded as a π-electron conjugated system, thus exhibiting semiconducting. On the other hand, as shown in Figure 1 (right), the peanut-shaped polymer has a coalesced structure via the general Stone-Wales rearrangement

Table 2
Classification of nanocarbon allotropes based on Gaussian curvature

π-electron system	Gaussian curvature	N-membered ring
graphene	0	6
fullerene	+	5,6
nanotubes	0(body) + (cap)	5,6
Mackay crystal* (hypothetical)	—	6,8
1D peanut-shaped polymers	+, —	5–8

*see Figure 13 (taken from Ref. 40).

(21,22) between adjacent C_{60} molecules. The EB-polymer can be regarded as a π-electron conjugated system, thus exhibiting metallic. In addition, when we focus on the geometrical aspect of the EB-polymer, this peanut-shaped structure has both positive and negative Gaussian curvatures (23), which are different from well-known π-electron conjugated nanocarbon allotropes (see Table 2).

In the present paper, we will introduce our recent works on the electron-transport (24), optical (25), and electronic properties (26,27) of the peanut-shaped C_{60} polymer with positive and negative Gaussian curvatures. In particular, we will discuss the effects of Gaussian curvatures on the electronic states of the polymer on the basis of the Schrodinger equation in Riemannian space (28,29). Finally, we will describe the perspective of the peanut-shaped C_{60} polymer from the viewpoint of topological science.

Experiments

Electron-transport Properties

To investigate the electron-transport properties of the peanut-shaped C_{60} polymer, we performed four-probe measurements in vacuum (24). After 12 hours of EB irradiation (applied voltage: 3 kV) of a C_{60} film (100 nm thick) deposited on a cesium iodide (CsI) substrate by sublimation of C_{60} powder (99.98% pure) at 673 K in a ultra-high vacuum (UHV) chamber (base pressure: 2×10^{-7} Pa) equipped with infrared spectroscopy, the film was taken out of the chamber and moved into the other vacuum chamber (base pressure: 4×10^{-4} Pa). Prior to a C_{60} film deposition on the CsI, the powder was preheated at 473 K until residual organic solvents were completely removed from the powder. Gold (Au) contacts were deposited on the peanut-shaped C_{60} polymer film through a metal mask, and the film resistance was recorded as a function of the substrate temperature in the range of 9–400 K.

Optical Properties

To investigate the optical properties of the peanut-shaped C_{60} polymer, we examined the dynamics of photo-excited carriers in the polymer, using two-color pump-probe femtosecond spectroscopy (a temporal resolution of 200 fs), in which a coaxial configuration between the pump (1.07 eV) and probe (1.55 eV) laser beams provides a high signal-to-noise ratio (S/N) (25,30). C_{60} films (200 nm thick) were formed on a CsI substrate in the UHV chamber described in the previous section by sublimation of the C_{60} powder at 673 K.

The peanut-shaped C_{60} polymer was prepared by 3 kV EB-irradiation, and its formation was confirmed using *in situ* infrared spectroscopy (31). We also prepared a pristine sample without EB irradiation as a reference. The films formed were mounted on the cold finger of an optical cryostat, and the lifetime of photo-excited carriers in the films was recorded as a function of the substrate temperature (20–300 K). The details of the measurement system and conditions were described in Ref. (25).

Electronic Structure

To clarify the origins of the metallic *I-V* characteristics of the peanut-shaped C_{60} polymer, we examined the valence electronic structure around the Fermi level (E_F), using *in situ* high-resolution ultraviolet photoemission spectroscopy (PES). Prior to a C_{60} film deposition, 100 mg of C_{60} powder (99.98% pure) introduced into a Knudsen cell (K–cell) was heated at 473 K for a few hours to remove residual organic solvents from the powder in a preparation chamber (base pressure: 1×10^{-7} Pa). Thereafter, a C_{60} film (20–30 nm thick) was formed on a copper (Cu) substrate by sublimation of the pretreated C_{60} powder in the K–cell at 673 K for 3 minutes in the preparation chamber. Subsequently, the pristine C_{60} film was transferred to an analysis chamber (base pressure: 1×10^{-8} Pa) and measured *in situ* by PES with an energy resolution of 12 meV and a monochromatic He Iα (21.218 eV) and/or IIα (40.806 eV) emission line. Although we used He Iα in Ref. (26), we used a He IIα emission line to examine the π-electron behavior near E_F for the outermost layers of the EB-irradiated film in Ref. (27). After the measurements, the film was returned to the preparation chamber and EB-irradiated for 0.5, 1.5, 2.5, 5.0, and 12 hours. We confirmed by *in situ* infrared spectroscopy that 12 hours of EB-irradiation was sufficient to allow the C_{60} molecules to completely coalesce, thus forming a peanut-shaped C_{60} polymer all over the film. After each EB-irradiation, the film was transferred to the analysis chamber for *in situ* PES measurements. The zero value in binding energy for the present measurements was determined from E_F ($= 0$ eV) of a Au film, which was deposited on the same Cu substrate as used for the pristine and EB-irradiated C_{60} films, by fitting its PES spectrum with a Fermi distribution function at the measurement temperature (350 K). In the present substrate temperature, E_F of a semiconductor was located in the middle between the valence and conduction bands by thermal broadening and was almost the same position as that of a metal with thermal broadening at the temperature.

Results and Discussion

Electron-transport Properties

We examined the temperature dependence of the electrical resistance of the peanut-shaped C_{60} polymer. Figure 2 shows the Arrehnius plot of the resistance of the polymer as a function of the substrate temperature. It was found that the electron–transport mechanism changed at around 90 K. For a substrate temperature above 90 K, the electron–transport was based on a thermally excited mechanism, and the activation energy of the electron conduction was obtained to be 60 meV, which is smaller than that of 100 meV for multi-walled carbon nanotubes (MWCNTs) (8). Because the peanut-shaped C_{60} polymer can be formed only by EB irradiation of a C_{60} film, which can be deposited on any substrate by dry (evaporation) or wet (spin coat) processes, this polymer can be superior to carbon nanotubes (CNTs) when applied to electronic devices. On the other hand, for a temperature below 90 K, although the electron–transport mechanism may change to a variable range

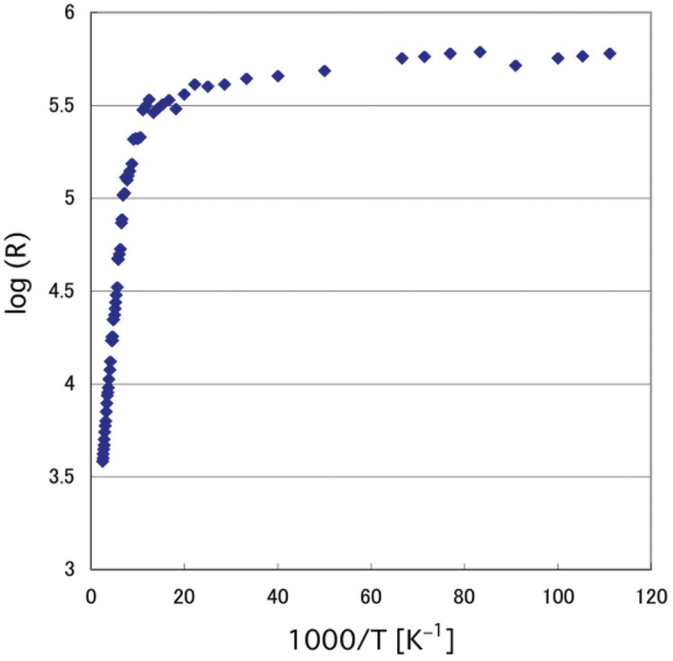

Figure 2. Arrehnius plot of the resistance of the peanut-shaped C_{60} polymer in the range of 9–400 K (taken from Ref. 24) (color figure available online).

hopping mechanism, *in situ* four-probe measurements are further needed to clarify whether or not the hopping mechanism is based on 1D metallic conduction, Mott–type, or Anderson localization.

Optical Properties

Typical transient $\Delta T(t)$, the difference in transmission from that of an equilibrium condition as a function of the delay time between the pump and probe pulses, for the peanut-shaped C_{60} polymer and pristine C_{60} films are shown in Figures 3(a) and 3(b), respectively. In the high temperature range exceeding 60 K, $\Delta T(t)$ was identical for both samples and showed an instantaneous response (hereafter called the "fast component"). This common feature remained largely unchanged over the whole temperature range. On the other hand, in the low temperature range below 60 K, $\Delta T(t)$ for the polymer sample showed an additional relaxation component with a slow decay (hereafter called the "slow component"), which became dominant in the low temperature range. It is noted that the fast component was still present even at the lowest temperature examined in the present work, though its outline was largely obscured by the slow component, as shown in Figure 3(a). As a result of considering the temperature-dependent (T-dependent) fast component (25), since the excitation energy of the incident pulses (pump: 1.07 eV, probe: 1.55 eV) was well below the optically allowed inter-band transitions of C_{60} molecules (17), the present observed instantaneous response can be attributed to two-photon absorption (TPA). In addition, the transmission change was found to be linearly dependent on the pump laser power, thus indicating that the signal consisted of a TPA process involving one pump photon and

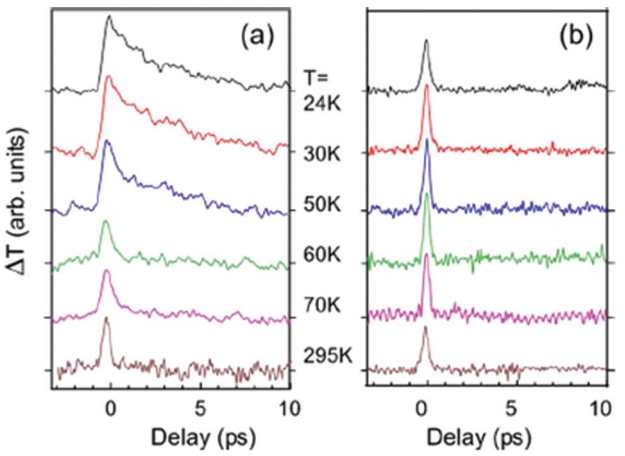

Figure 3. Typical transmission change ΔT(t) vs. decay time for (a) 1D peanut-shaped C_{60} polymer and (b) pristine C_{60} film over a wide temperature range of 20–300 K (taken from Ref. 25) (color figure available online).

one probe photon. This assignment agrees well with the transient profile, which is largely consistent with the correlation between the incident pulses.

We next consider the T-dependent slow component appearing at a lower temperature for the peanut-shaped C_{60} polymer. Using the two-component exponential decay function,

$$\Delta T(t) = A_f \exp(-t/\tau_f) + \mathrm{A}_s(T) \exp[-t/\tau_s(T)]$$

where A and τ, respectively, denote the amplitudes and relaxation times as a function of temperature, and the notations f and s refer to the fast and slow components, respectively. We obtained a good fit with the data of Figure 3(a) for the polymer sample. Because the fast component could be regarded as T-independent, A_f and τ_f were fixed at constant values throughout the fitting procedure. The results of $\tau_s(T)$ and $\mathrm{A}_s(T)$ obtained using the formula are shown in Figures 4(a) and 4(b), respectively. A signal with a decay time of a few picoseconds started to appear below 60 K and became dominant with further decreasing the temperature. A T-dependent transient signal with a similar decay time has been observed for various quasi-1D compounds (30,32), in which the appearance of relaxation bottleneck reflects an energy gap associated with a Peierls transition. Therefore, the slow component appearance indicates an energy gap formation below 60 K for the peanut-shaped C_{60} polymer in a similar manner to that for quasi-1D compounds, such as $K_{0.3}MO_3$. Consequently, the results of Figures 3 and 4 suggest that the peanut-shaped C_{60} polymer is a 1D or quasi-1D metallic carbon polymer.

Figures 5(a) and 5(b) show a schematic diagram of the transition processes accounting for the fast and slow transient components, respectively. For an excitation energy smaller than the inter-band energy gap, only the TPA process contributes to the $\Delta T(t)$, resulting in an instantaneous response during the correlation between the incident two pulses. The TPA transition is also applicable to the pristine sample. On the other hand, in the presence of a narrow energy gap, even when the gap includes large fluctuations, the photo-excited carriers from higher excited states to the gap states and vice versa contribute to the $\Delta T(t)$.

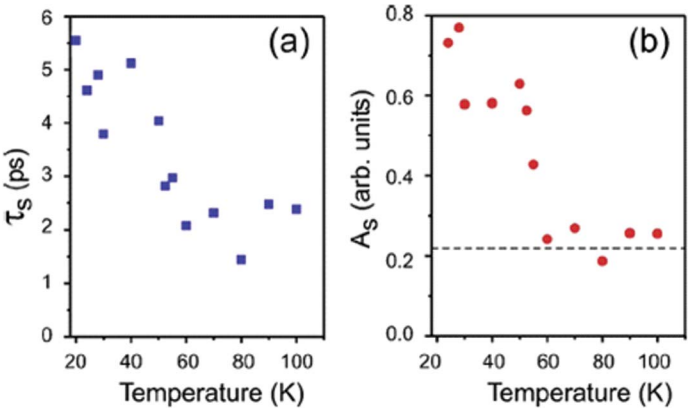

Figure 4. Temperature dependence of (a) decay time τ_s and (b) amplitude A_s for the slow component obtained from an exponential fitting to $\Delta T(t)$. The dashed line indicates the background level (taken from Ref. 25) (color figure available online).

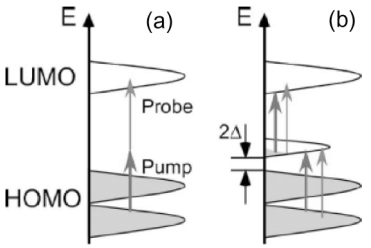

Figure 5. (a) Schematic diagram of a TPA process consisting of one pump photon and one probe photon. (b) Inter-band carriers relaxation processes in the presence of an energy gap at a lower temperature (taken from Ref. 25).

The T-dependent $\Delta T(t)$ reflects the T-dependence of the energy gap and order parameter fluctuations.

In typical quasi-1D compounds exhibiting the Peierls transition, the decay time diverges near the transition temperature at which efficient phonon transitions (both emissions and re-absorptions) greatly make the relaxation time longer at the beginning of the gap formation. However, as shown in Figure 4(a), there was no clear divergence at around 60 K, and instead the decay time and amplitude increased monotonically with decreasing temperature down to 20 K. We consider that the different behavior of the decay time is presumably due to a topological effect driven from the positive and negative Gaussian curvatures at present, but it is further necessary to study the present subject.

Electronic Properties

Figures 6 shows the PES spectra of the EB-irradiated C_{60} film for several irradiation times (350 K): 0 hour (red), 0.5 hour (orange), 1.5 hours (green), 2.5 hours (sky blue), and 5.0 hours (blue), along with that of the pristine C_{60} film measured at 300 K. For the pristine C_{60} film (red line), some intensive narrow bands such as HOMO and HOMO–1

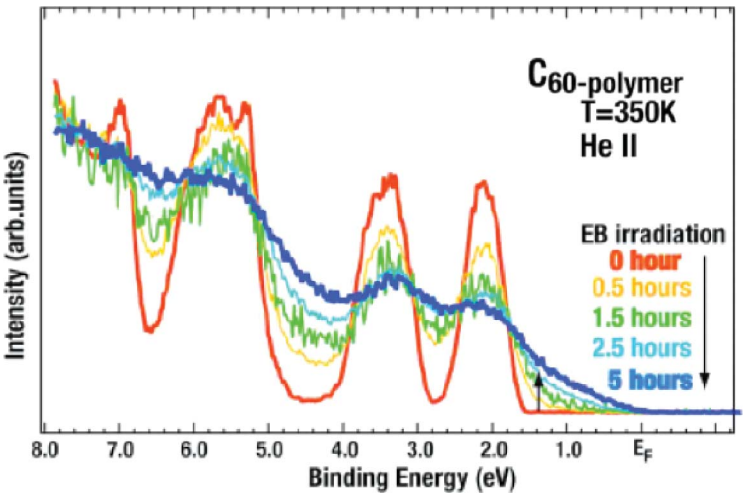

Figure 6. EB-time evolution of valence photoemission spectra of a C_{60} film in a wide binding energy region. All PES spectra were obtained at 350 K except that of pristine C_{60} film at 300 K (taken from Ref. 27) (color figure available online).

were observed because of the weak interaction between adjacent C_{60} molecules. On the other hand, as EB-irradiation time increased, each band became broadened in response to the disappearance of molecular character caused by EB-induced polymerization between adjacent C_{60} molecules, and the valence electronic states spread monotonically toward E_F with increasing EB-irradiation time. After 5 hours of EB-irradiation, the electronic states reached E_F, as illustrated by the blue line.

To understand this behavior near E_F in details, we next measured the EB-irradiation time–dependence of PES spectra of the film in the binding energy of 3 eV below E_F. Figure 7 shows the evolution of PES spectra of the C_{60} film in the binding energy region as a function of EB–irradiation time, where insets shows the spectra in the vicinity of E_F: 0 hour (red), 0.5 hour (orange), 2.5 hours (sky blue), and 5.0 hours (blue), which were symmetrized to remove the effect of thermal broadening from those own spectra. Because the S/N of the 1.5 hour-irradiated C_{60} film PES spectrum (the green line shown in Figure 7) was poor in comparison with that of the others, it was omitted in this figure. As shown in Figure 7, the electronic states in the binding energy range of 0–2 eV gradually increased in response to the broadening of the HOMO band located at around 2.4 eV as the EB-irradiation time increased. This indicates that EB-irradiation time reduced the energy gap, which is related to the electron-transport properties of a C_{60} film continuously. This finding implies that the electronic properties of a C_{60} film can be controlled from an insulator to a metal via a semiconductor continuously only within an EB-irradiated area, which is interesting when the EB-irradiated C_{60} polymer is applied to the fabrication of electronic devices.

Why did the electronic properties of the C_{60} film change continuously from insulating to metallic via semiconducting as EB irradiation time increased? One reason is attributed to the change in polymerization degree upon EB irradiation. We performed the first-principle calculations of the energy gap for the dimer (C_{60}-C_{60}), trimer (C_{60}-C_{60}-C_{60}), and one-dimensional system (-C_{60}-) with a give cross-linked structure between adjacent C_{60} molecules (18) and found them to be 0.33, 0.11, and 0.02 eV, respectively, along with

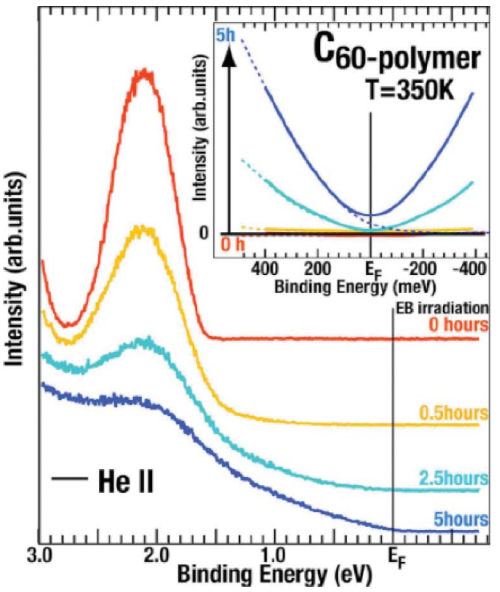

Figure 7. EB-time evolution of valence photoemission spectra of a C_{60} film in the binding energy of 3 eV below the Fermi level. Inset shows the symmetrized spectra in the vicinity of the Fermi level in order to remove the effect of thermal broadening (taken from Ref. 27) (color figure available online).

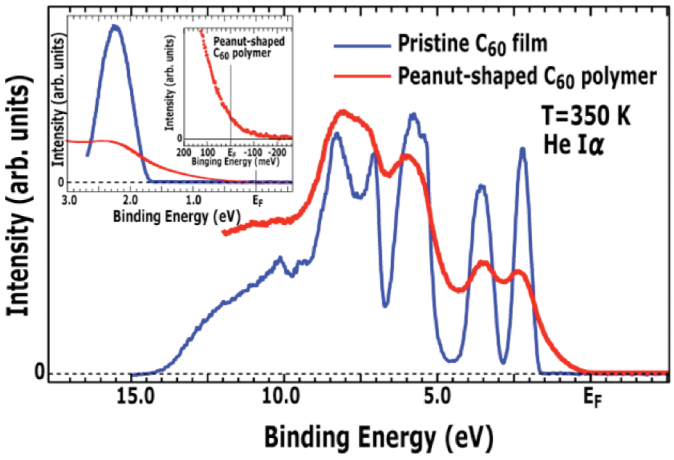

Figure 8. *In situ* high-resolution PES spectra of pristine C_{60} film (blue line) and 1D peanut-shaped C_{60} polymer (red line) obtained at 300 K and 350 K, respectively. Inset shows the PES spectrum of the 1D peanut-shaped C_{60} polymer near E_F (taken from Ref. 26) (color figure available online).

that of 1.67 eV for C_{60}, which is in an excellent agreement with experimental results of 1.6–1.8 eV (33). Another reason is attributed to the general Stone-Wales rearrangement between adjacent C_{60} molecules, which proceeded as EB irradiation time increased.

We next discuss the PES results obtained after 12-hour EB irradiation. Figure 8 shows PES spectra of pristine C_{60} (blue line) and peanut-shaped C_{60} polymer (red line) films obtained at a substrate temperature of 300 K and 350 K, respectively, where the inset shows

the PES spectrum of the peanut-shaped C_{60} polymer near E_F. For the peanut-shaped C_{60} polymer, each band was broadened in response to the disappearance of molecular character caused by EB-induced polymerization between adjacent C_{60} molecules, and the valence electronic states reached E_F. In order to clarify the behavior of the electronic structure of the peanut-shaped C_{60} polymer in the vicinity of E_F, we measured more precise PES spectra of the pristine C_{60} and peanut-shaped polymer films in the binding energy of 3.0 eV below E_F, as shown in the inset of Figure 8. It is found that the photoemission spectrum of the peanut-shaped polymer was much greater than that of the pristine C_{60} film near E_F and clearly came across E_F edge. These findings suggest that the peanut-shaped C_{60} polymer has a metallic electronic structure. However, the results shown in the inset of Figure 8 were measured at 350 K; thus, the effect of a thermal broadening on the PES spectra should be taken into account. This implies that it is possible that the peanut-shaped polymer is not only metal or semimetal but also a narrow-gap semiconductor.

We next examined the T-dependent PES spectra in the vicinity of E_F for the peanut-shaped C_{60} polymer because the thermal broadening effect reduces with decreasing temperature. For example, Figure 9 plots the Fermi distribution function near E_F in the range of 50–350 K (350 K: red, 200 K: orange, 150 K: green, 100 K: sky blue, and 50 K: blue) (34). At 350 K, there is a large thermal broadening in the distribution function in a similar manner to the spectrum shown in the inset of Figure 8. As temperature lowers from 350 K to 50 K, thermal broadening becomes smaller and the Fermi step at E_F appears clearly at 50 K, as shown in Figure 9. We examined the T-dependent PES spectra near E_F for the peanut-shaped C_{60} polymer. Figure 10 shows the PES spectra measured at 50 K (blue, top), 100 K (sky blue, second top), 150 K (green, middle), 200 K (orange, second bottom), and 350 K (red, bottom) (34). It is found that the spectrum came across E_F even at 50 K, thus indicating that the peanut-shaped polymer is metal. Interestingly, the spectral function does not clearly show a Fermi step even at 50 K, unlike the prediction shown in Figure 9. Two- and three-dimensional metal such as $TaSe_2$ and Rhodium, respectively, always exhibit a Fermi step, but quasi-1D metal such as $K_{0.3}MO_3$ and $(TaSe_4)I$ does not show such the step (35). Accordingly, the results of Figure 10 suggest that the

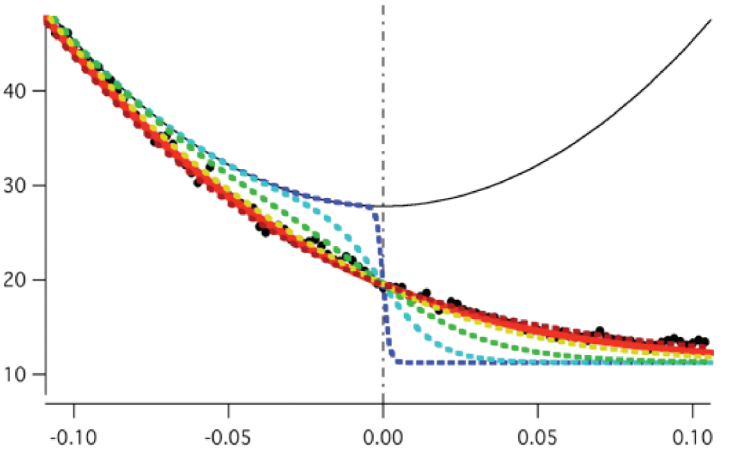

Figure 9. Plot of the Fermi distribution function as a function of temperature (red: 350 K, orange: 200 K, green: 150 K, sky blue: 100 K, and blue: 50 K) (taken from Ref. 34) (color figure available online).

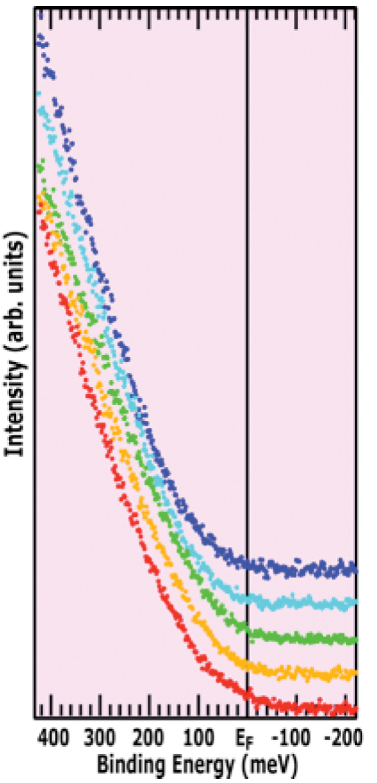

Figure 10. Temperature dependence of PES spectra in the vicinity of E_F: 350 K (red), 200 K (orange), 150 K (green), 100 K (skyblue), and 50 K (blue) (taken from Ref. 34) (color figure available online).

peanut-shaped C_{60} polymer is a 1D or quasi-1D metal, which is consistent with the results of the photo-excited carriers dynamics described in the previous section.

If the peanut-shaped polymer is 1D metal, the electrons should exhibit a Tomonaga-Luttinger liquids (TLL) behavior in which the density of states (DOS) shows a power-law dependence of the binding energy and temperature (the value of exponent α is less than unity) (36). For example, for metallic single-walled carbon nanotubes (SWCNTs), a TLL behavior is observed ($\alpha = 0.5$) (37), which is the direct evidence of 1D metal. In a similar manner to SWCNT, we examined the T-dependent PES spectra near E_F in the range of 30–350 K using a monochromatic He IIα emission line. We also observed a TLL behavior for both binding energy and temperature and obtained α to be ca. 0.6 (29), thus demonstrating that the peanut-shaped C_{60} polymer is 1D metal as well as SWCNTs. Here we have a next question: what is the difference in the exponent (α) value between SWCNT and the peanut-shaped polymer? Is the difference physically meaningful?

Riemannian Geometrical Effects on TLL Exponent

To understand the difference in the TLL exponent value between the SWCNT and peanut-shaped C_{60} polymer, we focused on the difference in their topology based on Gaussian curvature, as shown in Table 2. At the first step, we regarded the electron motion on the 1D

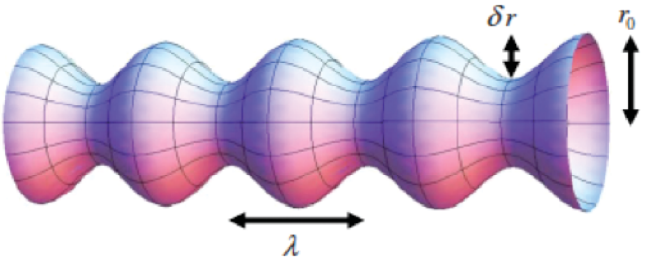

Figure 11. Schematic illustration of a quantum hollow cylinder with periodic radius modulation (taken from Ref. 28) (color figure available online).

peanut-shaped C_{60} polymer as free electrons moving on a quantum hollow cylinder with periodic radius modulation (see Figure 11), resulting in a 1D curved surface with positive and negative Gaussian curvatures aligned alternatively and periodically. On such the curved surface, the Schrodinger equation dealing with electron motion should be written not in Euclidean but rather in Riemannian space (28). As a consequence, the single-particle DOS, $n(\omega)$, near E_F exhibits a power-law singularity as follows:

$$n(\omega) \propto |\hbar\omega - E_F|^{\alpha}, \quad \alpha = \frac{K + K^{-1}}{2} - 1$$

Here, K (> 0) is a parameter to express the strength of electron-electron interactions and can be written as

$$K = \lim_{q \to 0} \sqrt{\frac{2\pi\hbar\upsilon_F + g_4(q) - g_2(q)}{2\pi\hbar\upsilon_F + g_4(q) + g_2(q)}}$$

Here, v_F denotes the Fermi velocity, and $g_4(q) = V(q, m)$ and $g_2(q) = V(q, m) - V(2k_F, m)$ are q-dependent coupling constants. $V(q, m)$ is the Fourier transform of the screened interaction. The details of the present theoretical treatments were described in Ref. (28). Figure 12 shows the δr dependence of both K and α for different k_F values. The insets in Figure 12 show the k_F dependence of K and α at $\delta r/a$ =2.0. Figure 12 demonstrates that K decreased and α increased significantly with increasing δr for $\delta r/a$ exceeding 2.5. Such δr-driven shifts in K and α are attributed to the effects of Gaussian curvatures on the nature of TLL states. Consequently, it is interesting to note that the difference in TLL exponent α value between SWCNT and 1D peanut-shaped C_{60} polymer can be explained by Riemannian geometrical effects.

Summary and Perspectives

We introduced our recent results of the electron-transport, optical, and electronic properties of the 1D uneven peanut-shaped C_{60} polymer formed by EB irradiation of C_{60} films. This polymer was found to be a 1D metal and can be regarded as a new allotrope of nanocarbon materials based on Gaussian curvature. Indeed, the 1D metallic polymer exhibits a different behavior of optical and electronic properties from well-known 1D metal materials: there is no divergence in the decay time upon an energy gap formation associated with the Peierls transition, and the TLL exponent value is larger than that of 1D metal SWCNT

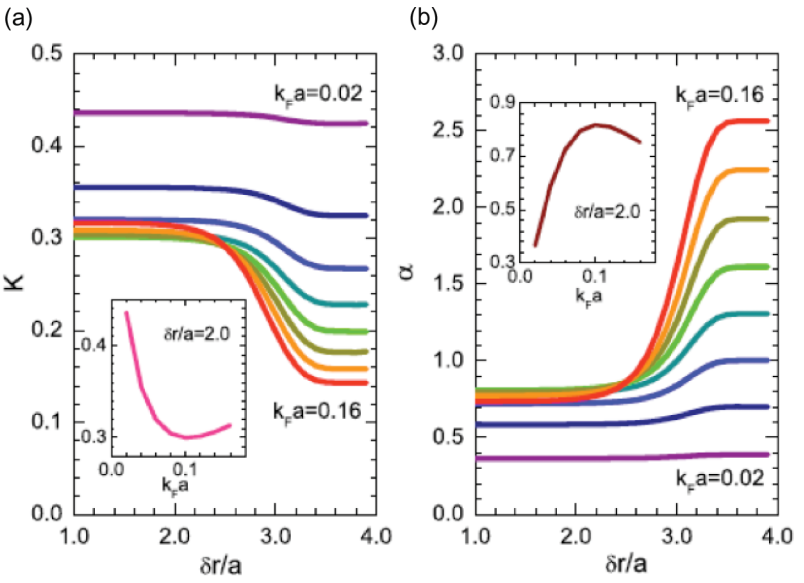

Figure 12. δr dependence of K and α defined by the equations described in section 3.4, respectively. Insets show nonmonotonic behaviors of K and α as a function of k_F at $\delta r/a$=2.0 (taken from Ref. 28) (color figure available online).

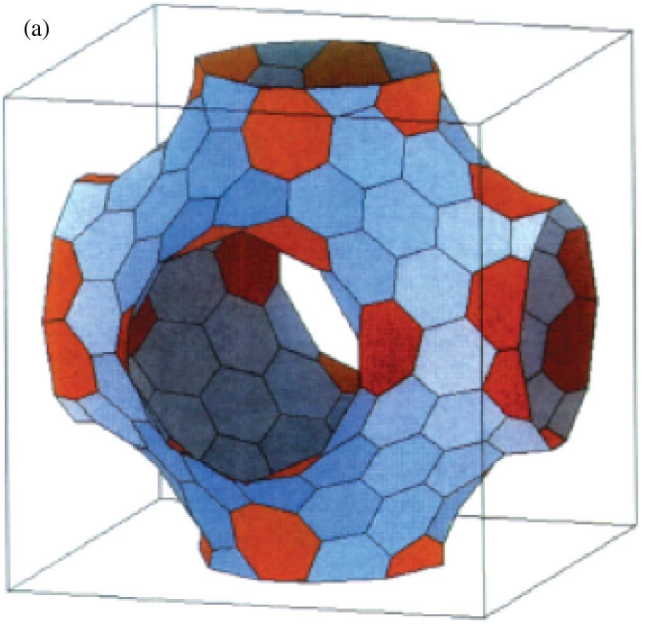

Figure 13. Schematic illustration of the unit cell of Mackay crystal consisting of 6- and 8-membered rings colored by blue and red, respectively (taken from Ref. 40) (color figure available online).

with zero Gaussian curvature. In particular, the increase in TLL exponent is caused by the Gaussian curvature that drives effective potentials acting on electrons motion along Riemannian surface.

There have been some reports on carbon materials with a negative Gaussian curvature experimentally (38–40). However, they were just observed using a transmission electron microscope, and their physical properties have not yet been examined. To the best of our knowledge, the 1D metallic uneven peanut-shaped C_{60} polymer is the first material with well-known physical properties that are affected by Riemannian geometry. Curvature effects on electronic, electric, and magnetic properties of condensates have been predicted theoretically (41–45), for example, so-called Mackay crystal shown in Figure 13 (41). We believe that the 1D uneven peanut-shaped C_{60} polymer is a good material to verify the theoretical predictions and open a new science in Riemannian space.

Acknowledgments

One of the authors (J.O.) is greatly thankful to PRESTO/CREST-JST, Murata Foundation, Sumitomo Foundation, and SCAT-Telcom for supporting the present studies financially. In addition, he also thanks Dr. S. Ryuzaki and Mr. A. Takashima for PES measurements.

References

1. Rao, A. M., Zhou, P., Wang, K.-A., Hager, G. T., Holden, J. M., Wang, Y., Lee, W.-T. et al. (1993) Photoinduced polymerization of solid C_{60} films. *Science*, 259: 955–957.
2. Onoe, J., Nakayama, T., Nakao, A., Hashi, Y., Esfarjani, K., Ohno, K., Kawazoe, Y., Aono, M., and Takeuchi, K. (2002) The nano-structure of C_{60} photopolymers. In *Clusters and Nanomaterials*, Springer-Verlag: Berlin, pp. 135–169, and references therein.
3. Onoe, J. and Takeuchi, K. (1996) In situ high-resolution infrared spectroscopy of a photopolymerized C_{60} film. *Phys. Rev. B*, 54: 6167–6171.
4. Onoe, J., Nakao, A., and Takeuchi, K. (1997) XPS study of a photopolymerized C_{60} film. *Phys. Rev. B*, 55: 10051–10056.
5. Onoe, J. and Takeuchi, K. (1997) How many [2+2] four-membered rings are formed on a C_{60} molecule when photopolymerization is saturated? *Phys. Rev. Lett.*, 79: 2987–2989.
6. Esfarjani, K., Hashi, Y., Onoe, J., Takeuchi, K., and Kawazoe, Y. (1998) Vibrational modes and IR analysis of neutral photopolymerized C_{60} dimers. *Phys. Rev. B*, 57: 223–229.
7. Nakayama, T., Onoe, J., Nakatsuji, K., Nakamura, J., Takeuchi, K., and Aono, M. (1999) Photo-induced products in a C_{60} monolayer on Si(111)$\sqrt{3}$x$\sqrt{3}$R30°-Ag : An STM study. *Surf. Rev. Lett.*, 6: 1073–1078.
8. Onoe, J., Nakayama, T., Nakao, A., Hashi, Y., Esfarjani, K., Kawazoe, Y., Aono, M., and Takeuchi, K. (2000) In situ FTIR, XPS, and STM studies of the nano-structure of a photopolymerized C_{60} film. *Mol. Cryst. Liq. Cryst*., 340: 689–694.
9. Onoe, J., Nakayama, T., Aono, M., and Hara, T. (2004) Electrical properties of a two-dimensionally hexagonal C_{60} photopolymer. *J. Appl. Phys*., 96: 443–445.
10. Hara, T., Onoe, J., and Takeuchi, K. (2000) In situ Fourier-transform infrared study of electron-irradiation-induced reaction in a C_{60} film. *Jpn. J. Appl. Phys.*, 39: 1872–1876.
11. Hara, T., Onoe, J., and Takeuchi, K. (2002) Field emission from an electron-beam irradiated C_{60} film. *J. Appl. Phys.*, 92: 7302–7305.
12. Onoe, J., Nakayama, T., Aono, M., and Hara, T. (2003) Structural and electrical properties of an electron-beam irradiated C_{60} film. *Appl. Phys. Lett*., 82: 595–597.
13. Hara, T. and Onoe, J. (2003) Vibrational analysis of peanut-shaped C_{120} fullerenes. *Eur. Phys. J. D*, 24: 389–392.

14. Onoe, J., Nakayama, T., Aono, M., and Hara, T. (2004) The electron transport properties of photo- and electron-beam-irradiated C_{60} films. *J. Phys. Chem. Solids*, 65: 343–348.
15. Onoe, J., Nakao, A., and Hida, A. (2004) Valence photoelectron spectra of an electron-beam irradiated C_{60} film. *Appl. Phys. Lett.*, 85: 2741–2743.
16. Beu, T. A., Onoe, J., and Hida, A. (2005) First-principle calculations of the electronic structure of one-dimensional C_{60} polymers. *Phys. Rev. B*, 72: 155416.
17. Ueda, S., Ohno, K., Noguchi, Y., Ishii, S., and Onoe, J. (2006) Dimension dependence of the electronic structure of fullerene polymers. *J. Phys. Chem. B*, 110: 22374–22381.
18. Beu, T. A. and Onoe, J. (2006) First-principles calculations of the vibrational spectra of one-dimensional C_{60} polymers. *Phys. Rev. B*, 74: 195426.
19. Wen, C., Li, J., Kitazawa, K., Aida, T., Honma, I., Komiyama, H., and Yamada, K. (1992) Electrical conductivity of a pure C_{60} single crystal. *Appl. Phys. Lett.*, 61: 2162–2163.
20. Mort, J., Ziolo, R., Machonkin, M., Huffman, D. R., and Ferguson, M. I. (1991) Electrical conductivity studies of undoped solid films of $C_{60/70}$. *Chem. Phys. Lett.*, 186: 284–286.
21. Stone, A. J. and Wales, D. J. (1986) Theoretical studies of icosahedral C_{60} and some related species. *Chem. Phys. Lett*., 128: 501–503.
22. Ueno, H., Osawa, S., Osawa, E., and Takeuchi, K. (1998) Stone-Wales rearrangement pathways from the hinge-opened [2+2] C_{60} dimer to IPR C_{120} fullerenes. Vibrational analysis of intermediates. *Fullerene Sci. Technol*., 6: 319–338.
23. "Gaussian curvature" is defined to be the product of the maximum and minimum curvatures at a given point on a curved surface.
24. Onoe, J., Ochiai, Y., Ito, T., Kimura, S., Ueda, S., Noguchi, Y., and Ohno, K. (2007) Electronic and electron–transport properties of peanut-shaped C_{60} polymers. *J. Phys. Conf. Ser*., 61: 899–903.
25. Toda, Y., Ryuzaki, S., and Onoe, J. (2008) Femtosecond carrier dynamics in an electron-beam-irradiated C_{60} film. *Appl. Phys. Lett.*, 92: 094102.
26. Onoe, J., Itoh, T., Kimura, S., Ohno, K., Noguchi, Y., and Ueda, S. (2007) In situ high-resolution photoelectron spectroscopic and density-functional study of a peanut-shaped C_{60} polymer. *Phys. Rev. B*, 75: 233410.
27. Onoe, J., Ito, T., and Kimura, S. (2008) Time dependence of the electronic structure of an electron-beam-irradiated C_{60} film. *J. Appl. Phys.*, 104: 103706.
28. Shima, H., Yoshioka, H., and Onoe, J. (2009) Geometry-driven shift in the Tomonaga-Luttinger exponent of deformed cylinders. *Phys. Rev. B*, 79: 201401(R).
29. Ito, T., Onoe, J., Shima, H., Yoshioka, H., and Kimura, S. (to be submitted).
30. Shimatake, K., Toda, Y., and Tanda, S. (2007) Selective optical probing of the charge-density-wave phases in $NbSe_3$. *Phys. Rev. B*, 75: 115120.
31. Onoe, J. and Takeuchi, K. (1995) In situ high-resolution FT-IR study of the orientational phase transition in C_{60} film. *J. Phys. Chem.*, 99: 16786–16791.
32. Demsar, J., Bijakovic, K., and Mihailovic, D. (1999) Single particle and collective excitations in the one-dimensional charge density wave solid $K_{0.3}MoO_3$ probed in real time by femtosecond spectroscopy. *Phys. Rev. Lett*., 83: 800–803.
33. Kremer, R. K., Rabenau, T., Maser, W. K., Kaiser, M., Simon, A., Haluska, M., and Kuzmany, H. (1993) High-temperature conductivity study on single-crystal C_{60}. *Appl. Phys. A*, 56: 211–214.
34. Onoe, J. (2009) Synthesis of new topological nanocarbons and their functional properties. In *Topology Designing*, NTS Publisher: Tokyo, pp. 312–324.
35. Dardel, B., Malterre, D., Grioni, M., Weibel, P., Baer, Y., and Levy, F. (1991) Unusual photoemission spectral function of quasi-one-dimensional metals. *Phys. Rev. Lett.*, 67: 3144–3147.
36. Voit, J. (1994) One-dimensional Fermi liquids. *Rep. Prog. Phys.*, 57: 977–1116.
37. For example Ishii, H., Kataura, H., Shiozawa, H., Yoshioka, H., Otsubo, H., Takayama, Y., Miyahara, T. et al. (2003) Direct observation of Tomonaga-Luttinger liquid state in carbon nanotubes at low temperatures. *Nature*, 426: 540.

38. Luzzi, D. E. and Smith, B. W. (2000) Carbon cage structures in single wall carbon nanotubes: a new class of materials. *Carbon*, 38: 1751–1756.
39. Terrones, M., Banhart, F., Grobert, N., Charlier, J.-C., Terrones, H., and Ajayan, P. M. (2002) Molecular junctions by joining single-walled carbon nanotubes. *Phys. Rev. Lett.*, 89: 075505.
40. Nasibulin, A. G., Pikhitsa, P. V., Jiang, H., Brown, D. P., Krasheninnikov, A. V., Anisimov, A. S., Queipo, P. A. et al. (2007) A novel hybrid carbon material. *Nature Nanotech.*, 2: 156–161.
41. Mackay, A. L. and Terrones, H. (1991) Diamond from graphite. *Nature*, 352: 762.
42. Townsend, S. J., Lenosky, T. J., Muller, D. A., Nichols, C. S., and Elser, V. (1992) Negatively curved graphite sheet model of amorphous carbon. *Phys. Rev. Lett*., 69: 921–924.
43. Park, N., Yoon, M., Berber, S., Ihm, J., Osawa, E., and Tomanek, D. (2003) Magnetism in all-carbon nanostructures with negative Gaussian curvature. *Phys. Rev. Lett.*, 91: 237204.
44. Terrones, H. and Terrones, M. (2003) Curved nanostructures materials. *New J. Phys.*, 5: 126.1–126.37.
45. Taira, H. and Shima, H. (2007) Electronic states in cylindrical surfaces with local deformation. *J. Phys. Conf. Ser.*, 61: 1142–1146.